Geophysical Research Letters

RESEARCH LETTER
10.1029/2023GL103894

Plasma Wave and Particle Dynamics During Interchange Events in the Jovian Magnetosphere Using Juno Observations

A. Daly[1], W. Li[1], Q. Ma[1,2], X.-C. Shen[1], P. H. Yoon[3], J. D. Menietti[4], W. S. Kurth[4], G. B. Hospodarsky[4], B. H. Mauk[5], G. Clark[5], F. Allegrini[6,7], J. E. P. Connerney[8], and S. J. Bolton[6]

[1]Center for Space Physics, Boston University, Boston, MA, USA, [2]Department of Atmospheric and Oceanic Sciences, University of California, Los Angeles, Los Angeles, CA, USA, [3]Institute for Physical Science and Technology, University of Maryland, College Park, MD, USA, [4]Department of Physics and Astronomy, University of Iowa, Iowa City, IA, USA, [5]The Johns Hopkins University Applied Physics Laboratory, Laurel, MD, USA, [6]Southwest Research Institute, San Antonio, TX, USA, [7]University of Texas at San Antonio, San Antonio, TX, USA, [8]Goddard Space Flight Center, Greenbelt, MD, USA

Abstract Interchange instability is known to drive fast radial transport of particles in Jupiter's inner magnetosphere. Magnetic flux tubes associated with the interchange instability often coincide with changes in particle distributions and plasma waves, but further investigations are required to understand their detailed characteristics. We analyze representative interchange events observed by Juno, which exhibit intriguing features of particle distributions and plasma waves, including Z-mode and whistler-mode waves. These events occurred at an equatorial radial distance of ~9 Jovian radii on the nightside, with Z-mode waves observed at mid-latitude and whistler-mode waves near the equator. We calculate the linear growth rate of whistler-mode and Z-mode waves based on the observed plasma parameters and electron distributions and find that both waves can be locally generated within the interchanged flux tube. Our findings are important for understanding particle transport and generation of plasma waves in the magnetospheres of Jupiter and other planetary systems.

Plain Language Summary The centrifugal interchange instability, which has been observed in rapidly rotating planets, like Saturn and Jupiter, moves cold plasmas inside of the magnetosphere further away, and transports hotter, less dense plasmas toward the inner magnetosphere. These moving flux tubes have been observed at Jupiter together with plasma waves, but their detailed characteristics are not fully understood. In the present study, we use observations from the Juno spacecraft to report multiple representative interchange events and evaluate the properties of energetic particles and plasma waves. Furthermore, we use linear theory to calculate the growth rates of Z-mode and whistler-mode waves during these events. Our findings reveal the typical features of plasma waves and particles during interchange events, which provide important insights into particle transport and generation of plasma waves at Jupiter and possibly other magnetized planets in our solar system and beyond.

Key Points:

- Several plasma transport events associated with interchange instability are identified alongside plasma waves using Juno observations
- Linear growth rate analyses indicate that waves can be locally generated during interchange events due to anisotropic electron distributions
- Our findings provide insights into electron transport and plasma wave dynamics during interchange events in planetary magnetospheres

Supporting Information:

Supporting Information may be found in the online version of this article.

Correspondence to:

A. Daly and W. Li,
adaly@bu.edu;
wenli77@bu.edu

Citation:

Daly, A., Li, W., Ma, Q., Shen, X.-C., Yoon, P. H., Menietti, J. D., et al. (2023). Plasma wave and particle dynamics during interchange events in the Jovian magnetosphere using Juno observations. *Geophysical Research Letters*, *50*, e2023GL103894. https://doi.org/10.1029/2023GL103894

Received 30 MAR 2023
Accepted 29 JUN 2023

1. Introduction

The centrifugal interchange instability involves the process where magnetic flux tubes containing cold, dense plasmas from the inner magnetosphere are interchanged with flux tubes consisting of hot, tenuous plasmas found farther out in the magnetosphere (Azari, 2020; Thomsen, 2013). Jupiter's rapidly rotating magnetosphere induces an outward centrifugal force, and the regions with a local gradient in flux tube content may be subject to interchange instability (Ma et al., 2016; Thomsen et al., 2015).

Interchange instability is recognized to play an important role in mass and plasma transport in Jupiter's magnetosphere (Dumont et al., 2014; Rymer et al., 2009; Southwood & Kivelson, 1987). Flux tubes associated with the interchange instability exhibit distinct features, such as sharp density cavities, as well as abrupt changes in magnetic field and particle fluxes (e.g., Bolton et al., 1997; Kivelson et al., 1997; Thorne et al., 1997). Particles within the interchanged flux tubes undergo gradient and curvature drifts, providing valuable information to determine the age, speed, and source region of injections in association with the interchange instability (Burch et al., 2005; Hill et al., 2005; Paranicas et al., 2020). These injections are called "interchange injections" hereafter. Interchange injections are characterized by enhancements in energetic particle fluxes, a depletion in low-energy particle fluxes, and enhanced wave activity and magnetic pressure (e.g., Azari et al., 2018; Burch et al., 2005; Chen & Hill, 2008; Hill et al., 2005; Kennelly et al., 2013; Rymer et al., 2009). At Saturn, interchanged flux tubes

have been found to be associated with various plasma waves, including enhanced electron cyclotron harmonic (ECH) waves, whistler-mode emissions, and upper hybrid emissions (e.g., Kennelly et al., 2013). Galileo observations at Jupiter revealed rapid inward interchange events in the Io torus, where the detected flux tubes exhibited enhanced whistler-mode waves and significant changes in electron distributions (Bolton et al., 1997; Kivelson et al., 1997; Thorne et al., 1997). Recently, using Juno observations at Jupiter, Kurth et al. (2023) found that injections near the Io torus are associated with quasi-electrostatic wave intensifications. Moreover, recent studies using multifluid plasma simulations have shown that Saturn-like exoplanets with rapid rotation may experience centrifugal interchange instabilities when located at a considerable distance from their host star (Tilley et al., 2016). These findings highlight the potential for interchange instabilities to occur in planetary systems beyond our solar system.

In this letter, we focus on two plasma wave modes, Z-mode and whistler-mode waves, during interchange events at Jupiter. The Z-mode wave is an electromagnetic wave trapped between the left-hand cutoff frequency ($f_{L=0}$) and the upper hybrid frequency (f_{uh}). The polarization of Z-mode waves switches at the electron plasma frequency (f_{pe}), with waves propagating below being left-hand polarized and waves above f_{pe} being right-hand polarized. The generation mechanism of Z-mode waves is suggested to be electron cyclotron maser instability (Wu & Lee, 1979; Yoon et al., 1998). Z-mode waves are typically observed near the polar region (Kaiser et al., 1993) and at middle latitudes at M-shell $< \sim 10$ (Menietti et al., 2021), where M-shell is defined as the radial distance in Jovian radii from the equatorial crossing of a magnetic field line to Jupiter's center. However, the generation and source region of Z-mode emissions, especially during interchange events, remain unresolved questions.

In comparison, whistler-mode waves are electromagnetic emissions that appear below electron cyclotron frequency (f_{ce}). Jovian whistler-mode chorus waves are generated near the equator and typically form in two bands: a lower band over 0.1–0.5 f_{ce} and an upper band over 0.5–1 f_{ce} (Hospodarsky et al., 2012). Whistler-mode chorus waves in the magnetosphere are known to be generated due to anisotropic distributions of electrons (Kennel, 1966; Li et al., 2008). Whistler-mode waves are observed in an extensive region from the equator to high magnetic latitudes at M-shells from 6 to 13 at Jupiter (Li et al., 2020; Menietti et al., 2021). However, similar to Z-mode emissions, the detailed generation mechanism during interchange events is not well understood.

In the present study, we analyze multiple interchange events at Jupiter using Juno data (Bolton, 2010). To evaluate the relationship between interchange events and plasma waves, we conducted a quantitative analysis of two specific events. To determine whether the plasma waves are generated within the interchanged flux tube, we calculated the linear growth rates and compared them with the observed wave data.

2. Observations of Interchange Events by Juno

The particle, plasma wave, and magnetometer instruments onboard Juno are used to evaluate the properties of energetic electrons, ions, and plasma waves during interchange events. The Waves instrument is used to obtain wave magnetic properties from ∼50 Hz to ∼20 kHz and wave electric properties from ∼50 Hz to ∼150 kHz (Kurth et al., 2017). The Jovian Auroral Distributions Experiment (JADE) measures the low energy electrons from below 0.1 to 100 keV and ions from ∼5 eV to ∼50 keV (McComas et al., 2017). The Jupiter Energetic Particle Detector Instrument (JEDI) measures the high-energy component of electrons from ∼25 keV to ∼1 MeV and ions from 10 s of keV to >1 MeV (Mauk et al., 2017). Particle cyclotron frequencies are calculated through the in situ magnetic field measurements from the Magnetic Field Investigation instrument (Connerney et al., 2017), and are used to identify relevant wave modes in this study.

2.1. Z-Mode Wave Events

Particle and wave measurements were recorded during an interchange event that occurred on 17 February 2020 (perijove 25, or PJ-25) between 12:24:00 and 12:25:30 UT (Figure 1). During this event, an intensification of Z-mode waves was observed at a radial distance corresponding to M-shell of ∼9.2, on the nightside with a magnetic local time (MLT) of 23.1 hr, and near the magnetic equator with a magnetic latitude (MLAT) of 23.1°. During this period, Juno detected a rapid increase in the magnetic field within the interchange event, with positive and negative spikes in the rate of change (dB/dt) about 1–1.5 nT/s at the boundaries. Meanwhile, JEDI (Figure 1b) and JADE (Figure 1c) measurements show sudden increases in electron flux from 100 s of eV to ∼200 keV and a rapid decrease in electron flux below ∼100 eV. Figures 1d and 1e show pitch angle distributions of electron fluxes

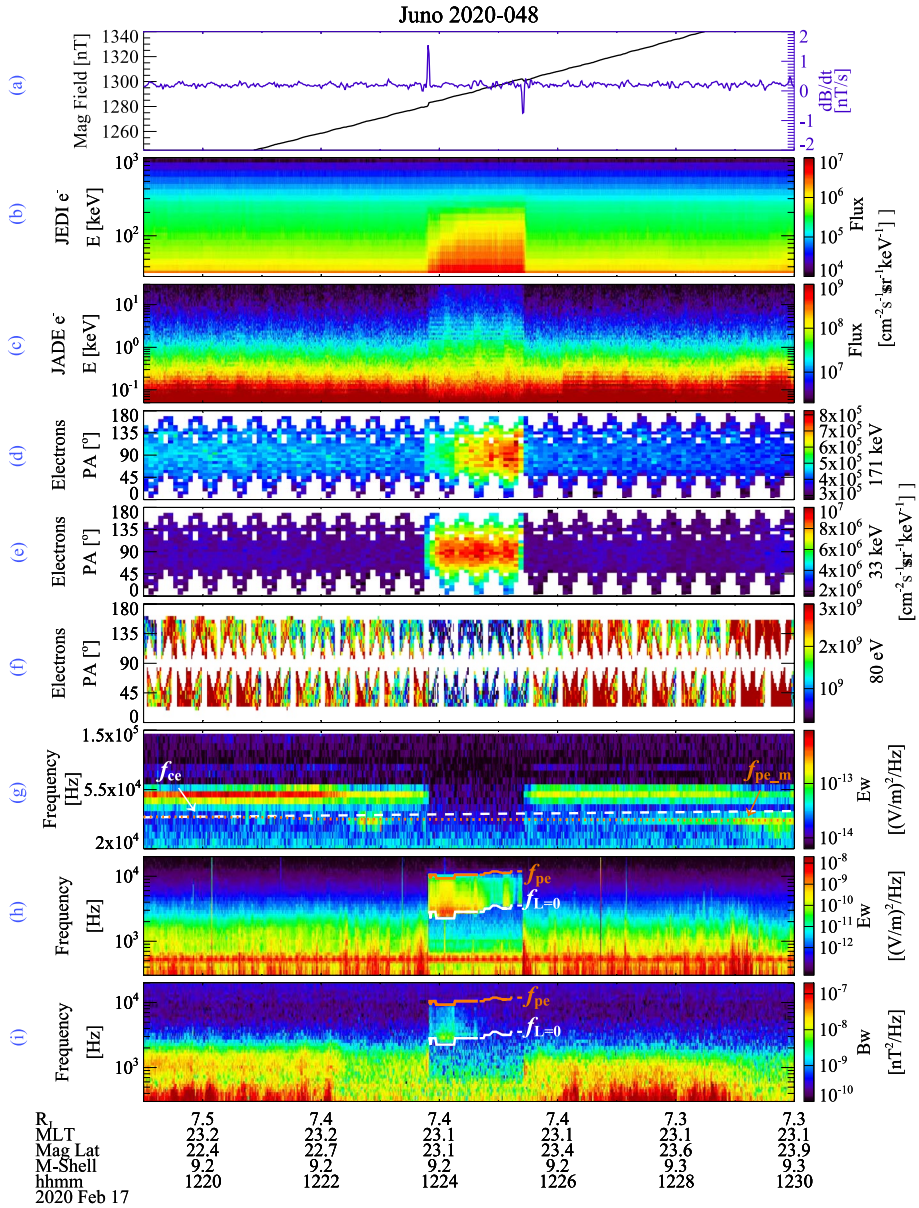

Figure 1. Juno observations of energetic electrons and plasma waves on 17 February 2020. (a) Magnetic field strength (black) and rate of change (dB/dt, blue); (b) Energy spectrogram of electron fluxes observed by JEDI, and (c) JADE; (d–f) Pitch angle distributions of electron fluxes at 171 keV, 33 keV, and 80 eV; (g) Wave electric spectrogram at frequencies from 20 to 150 kHz; (h–i) Wave electric and magnetic field power spectrograms at frequencies from 300 Hz to 20 kHz, where the white dashed line is the local electron gyrofrequency, the white solid line is the left-hand cutoff frequency ($f_{L=0}$), the orange dotted line is the modeled plasma frequency, and the orange solid line is the calculated plasma frequency based on $f_{L=0}$.

at 171 and 33 keV, respectively. While there was an increase in flux, the electrons also exhibited an increase in pitch angle anisotropy, shifting from an isotropic distribution outside of the event to a pancake distribution (with a peak in electron flux near 90° pitch angle) inside of the event. This increased anisotropy in association with a flux increase in high energy electrons, which is likely attributed to betatron acceleration (Mitchell et al., 2015), supports the scenario of inward radial transport (Bolton et al., 1997). At the lowest energy channels (~80 eV), the electron flux decreased rapidly inside of the event (Figure 1f). The proton flux suddenly increased at an energy of 9 keV (and up to ~1 MeV) inside of the interchange event, as shown in Figure S1 in Supporting Information S1.

Inside of the interchange event, Z-mode waves were detected over 2.5–10 kHz with the lower cutoff frequency at $f_{L=0}$, as expected for a left-hand polarized Z-mode wave (Figures 1h and 1i). Using the equation of $f_{pe} = \sqrt{f_{L=0}(f_{L=0} + f_{ce})}$,

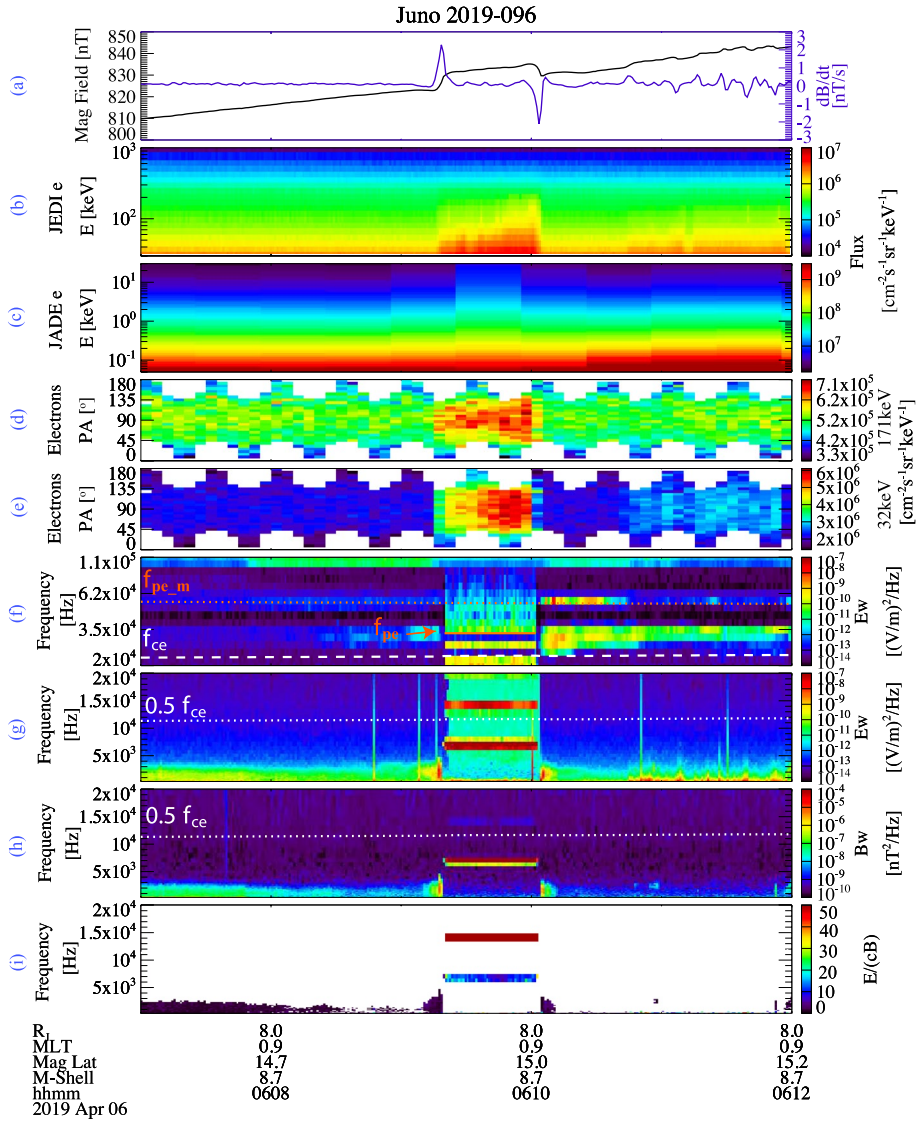

Figure 2. Similar format to Figure 1 but during 06:07–06:12 UT on 6 April 2019. In panels (g–h), the white dotted line is half of the local electron cyclotron frequency. (i) The ratio between the wave electric and magnetic fields.

we calculated f_{pe} (as marked by the orange solid line in Figures 1h and 1i) based on the identified $f_{L=0}$ and the electron cyclotron frequency (f_{ce}) calculated from the in situ magnetic field measurements. The modeled plasma frequencies outside of events (f_{pe_m}) in Figures 1g and 2f were derived from an empirical 2D density model from Dougherty et al. (2017), which used plasma parameters from Bagenal et al. (2017) based on measurements from the Voyager Plasma Science Instrument. The intensified wave emissions at ∼55 kHz in Figure 1g and ∼62 kHz in Figure 2f outside of the interchange events are most likely at the upper hybrid resonance frequency, which is consistent with the modeled upper hybrid frequency (not shown) calculated based on the modeled plasma frequency and the electron cyclotron frequency. These density estimates are essential for calculating wave growth rates. Compared to f_{pe_m}, the inferred f_{pe} from the wave spectral feature suddenly dropped at the onset of the interchange event. Based on $f_{pe} \approx 8980\sqrt{n_e}$ Hz, the total electron density is approximately 1.8 cm^{-3} inside of the event (12:24:30 UT), whereas it is 13.7 cm^{-3} outside of the event (at 12:22:15 UT), indicative of an inward moving flux tube. The Z-mode wave power was more evident in electric spectral density (Figure 1h) than that in magnetic spectral density (Figure 1i). The calculated Z-mode wave magnetic wave amplitude (integrated from 1.59 to 11.2 kHz) peaks at 4.1 pT.

Another example of an interchange event associated with Z-mode waves is shown in Figure S2 in Supporting Information S1. This event occurred at an *M*-Shell of 8.7, MLAT of 31.7°, and MLT of 2.4 hr. Juno detected two

interchange events which exhibited a rapid increase in magnetic field strength, an increase in electron flux from 100 s of eV to several hundred keV, an increase in proton fluxes up to a few hundred keV (Figure S3 in Supporting Information S1), and a depletion in electron density in association with Z-mode wave intensification. These features are very similar to Figure 1, suggesting that these features may occur often at $M \sim 9$ and middle latitudes (>20°), but further investigations are required to confirm these findings.

2.2. Whistler-Mode Wave Events

On 6 April 2019 (PJ-19), whistler-mode chorus waves were intensified during an interchange event (Figure 2). This event occurred from 06:09:20 to 06:10:10 UT at $M \sim 8.7$, MLAT ~ 15°, and MLT ~ 0.9 hr. At the onset of the interchange event (06:09:20 UT), the magnetic field intensity sharply increased, followed by a rapid decrease at the end of the event (Figure 2a). JADE and JEDI instruments measured sudden flux enhancements up to over 200 keV (Figures 2b and 2c). Due to the lower time resolution of the JADE data during this event, the sudden increase in electron flux is not as evident as in the JEDI data. The electron pitch angle distributions at 171 keV (Figures 2d) and 32 keV (Figures 2e) indicate that the distribution was more isotropic outside of the interchange event but changed to a more evident pancake distribution inside of the event.

During this event, two bands of chorus waves were detected near 7 kHz (lower band) and 14 kHz (upper band) along with ECH waves observed at frequencies near 28 kHz (Figure 2f). The lower band chorus wave was strongly electromagnetic and had a narrow frequency band at ~7.08 kHz and a magnetic wave amplitude (integrated from 5 to 7.96 kHz) of 861 pT, much stronger than whistler-mode waves observed by Juno in previous surveys (Li et al., 2020; Menietti et al., 2021). However, the upper band chorus had little magnetic wave power, indicative of quasi-electrostatic waves, as shown in the ratio between the wave electric and magnetic fields (Figure 2i). The lower cutoff of the intensified wave at ~35 kHz inside of the event in Figure 2f is assumed to be the electron plasma frequency, corresponding to the in situ total electron density of 13.5 cm^{-3}. However, the modeled density based on Dougherty et al. (2017) outside of the event (at 06:08:15 UT) is approximately 37.5 cm^{-3}. The observed features of the sharp increase in magnetic field strength, a rapid increase in electron flux up to 200 keV, and a decrease in electron density suggest that this magnetic flux tube is likely transported radially inward from outside. It is noteworthy that proton flux also exhibits increases at higher energies (>~10 keV) but decreases at lower energies (<~10 keV), as shown in Figure S4 in Supporting Information S1.

Another representative interchange event associated with whistler-mode waves was observed on the same day, as shown in Figures S5 and S6 in Supporting Information S1. This event, which occurred at $M \sim 9.3$, MLAT ~ 9.1°, and MLT ~ 0.8 hr, had a short duration, as shown by the repeated sudden increases and drops in magnetic field strength ranging from 3 to 13 nT. This interchange event was also characterized by an increase in electron flux from 10 to ~150 keV and a decrease in electron flux below 10 keV (Figure S5 in Supporting Information S1). However, the changes in proton flux were not very evident (Figure S6 in Supporting Information S1), possibly due to a smaller radial gradient in flux for protons than electrons in Jupiter's near-equatorial magnetosphere (Kollmann et al., 2017).

3. Growth Rate Analysis

To evaluate whether the observed Z-mode and whistler-mode waves are locally generated, we calculate the linear growth rates of waves inside and outside of the interchange events, as shown in Figures 1 and 2, based on the measured plasma parameters and electron distributions.

3.1. Z-Mode Waves

The Z-mode wave was marked between $f_{L=0}$ and f_{pe}, as shown in Figure 1. The total electron density of this event is estimated to be 1.8 cm^{-3} with an ambient magnetic field strength near 1,290 nT, and f_{pe}/f_{ce} ratio of 0.29. The relativistic temporal growth/damping rate (γ_w) is derived through the linear dielectric tensor (e.g., Yoon and Krauss-Varban, 1990) based on the cyclotron maser instability,

$$\gamma_w = \frac{\pi}{2\omega}\frac{4\pi n e^2}{(1+T^2)R}\int d\boldsymbol{p}\sum_{s=-\infty}^{\infty}\left\{\frac{\gamma\omega}{\Omega}\left[K\sin\theta + T\left(\cos\theta - \frac{kv_\parallel}{\omega}\right)\right]\frac{J_s(b)}{b} - J_s'(b)\right\}^2$$
$$\times\,\delta\left(\omega - \frac{s\Omega}{\gamma} - kv_\parallel\cos\theta\right)\left(\frac{s\Omega}{\gamma v_\perp}\frac{\partial}{\partial \boldsymbol{p}_\perp} + k\cos\theta\frac{\partial}{\partial \boldsymbol{p}_\parallel}\right) f\left(\boldsymbol{p}_\perp^2, \boldsymbol{p}_\parallel\right).$$

here $p_\parallel$ and $p_\perp$ are the electron momentum parallel and perpendicular to the magnetic field ($\boldsymbol{p} = \gamma m \boldsymbol{v}$), γ is the Lorentz factor, θ is the angle of propagation for the wave phase velocity, $J_s(b)$ and $J_s'(b)$ are the Bessel function and its first derivative with argument $b = k_\perp v_\perp \gamma / \Omega$, k and ω are the wavenumber and angular frequency, $\Omega = eB/mc$ is the angular electron cyclotron frequency, n and m are the electron number density and mass, and $f\left(p_\perp^2, p_\parallel\right)$ is the electron phase space density (PSD) distribution as a function of momentum. Equations for the parameters R, T, and K can be found in Text S1 in Supporting Information S1.

The pitch angle distribution in Figure 3a exhibits a peak in electron PSD at 90° for most JEDI energy channels, and a more isotropic distribution outside of the event (Figure 3e). The electron PSD was fitted with a polynomial filter (see more details in Text S2 in Supporting Information S1) and is shown in a polar plot of pitch angle and energy in Figures 3b and 3f. The fitted energy distribution reveals some anisotropies at high energies at pitch angles near the loss cone (Figure 3b). The calculated temporal growth rate of Z-mode waves indicates positive values at 0.15–0.25 f_{ce} (Figure 3c) over the wave normal angles of 90–150°. The maximum normalized growth rate of $\gamma/\Omega_{max} = 8.5 \times 10^{-6}$ (among all wave normal angles) is converted to convective growth rate as 3.4 dB per Jovian radii (dB/R_J) (Chen et al., 2010), as shown in Figure 3d (blue line). This frequency range corresponding to the positive wave growth is roughly consistent with the observed wave spectra (black line), suggesting that the Z-mode waves are likely generated locally within the flux tube.

Outside of the event, at 12:22:15 UT, the f_{pe}/f_{ce} ratio is 0.94. With no clear anisotropies for the electron distributions (Figure 3f), there is no positive wave growth (Figure 3g), consistent with the Juno observations (Figure 3h).

3.2. Whistler-Mode Wave Growth

The whistler-mode waves shown in Figures 2g and 2h are electromagnetic lower band chorus wave with a peak intensity at 0.3 f_{ce} and quasi-electrostatic upper band chorus wave with a peak intensity above 0.5 f_{ce}. The electron density during this event was estimated to be 13.5 cm^{-3}, while the ambient magnetic field strength was 833 nT. We calculate the linear growth rate of whistler-mode waves based on Equation 3.9 in Kennel (1966) using the linear wave instability code developed by Ma et al. (2014) using the formula shown in previous studies (e.g., Chen et al., 2010; Xiao et al., 1998, 2003).

Inside of the interchange event, electrons exhibited an anisotropic distribution (Figure 4a) with a large PSD gradient near 135° pitch angle, favorable for whistler-mode wave generation. However, outside of the interchange event, the electron pitch angle distribution was more isotropic (Figure 4e). The electron PSD was fitted with a polynomial filter and is shown in Figures 4b and 4f. The growth rate calculations show positive values in a narrow band over 0.24–0.28 f_{ce}, with a maximum normalized growth rate of 6.27×10^{-5} (Figure 4c), or convective growth rate of 45.41 dB/R_J, at 0.26 f_{ce} at 0° wave normal angle. These results are consistent with the wave measurements by Juno (Figure 4d), where the chorus wave had a narrow band over the similar frequency range, again suggesting that these whistler-mode waves are generated locally within the flux tube. It is noteworthy that no positive growth rate was obtained at the upper band above 0.5 f_{ce}, which is inconsistent with the observation (Figure 2h). This is probably because the minimum resonant energy corresponding to the upper band is 23.5 keV, which is below the lower energy limit of the JEDI electron measurement.

Outside of the event, at 06:08:15 UT, the density was approximately 37.5 cm^{-3}, and the magnetic field strength was 818 nT. At this time, the pitch angle distribution was mostly isotropic (Figure 4e), which can also be seen in the electron distribution in Figure 4f. Therefore, there is no positive growth rate (Figure 4g), which is consistent with the Juno wave observations (Figure 4h).

4. Summary and Discussion

By utilizing particle and plasma wave data from Juno, we report four representative examples of interchange events, during which Z-mode or whistler-mode waves were intensified. We calculated the linear growth rates based on the observed plasma parameters and electron distributions. The major findings are summarized below.

1. The reported two interchange events associated with Z-mode waves occurred near M-shell ~9, at mid-latitudes (MLATs of 23.1° and 31.5°), and near the nightside (MLTs of 23.1 and 2.4 hr). Both events are indicative of inward radial transport, characterized by a rapid increase in magnetic field strength, an increase in electron flux from a few hundred eV to hundreds of keV, a decrease in electron flux below a few hundred eV, and a substantial decrease in total electron number density coincided with the intensification of Z-mode waves inside of the interchange events.

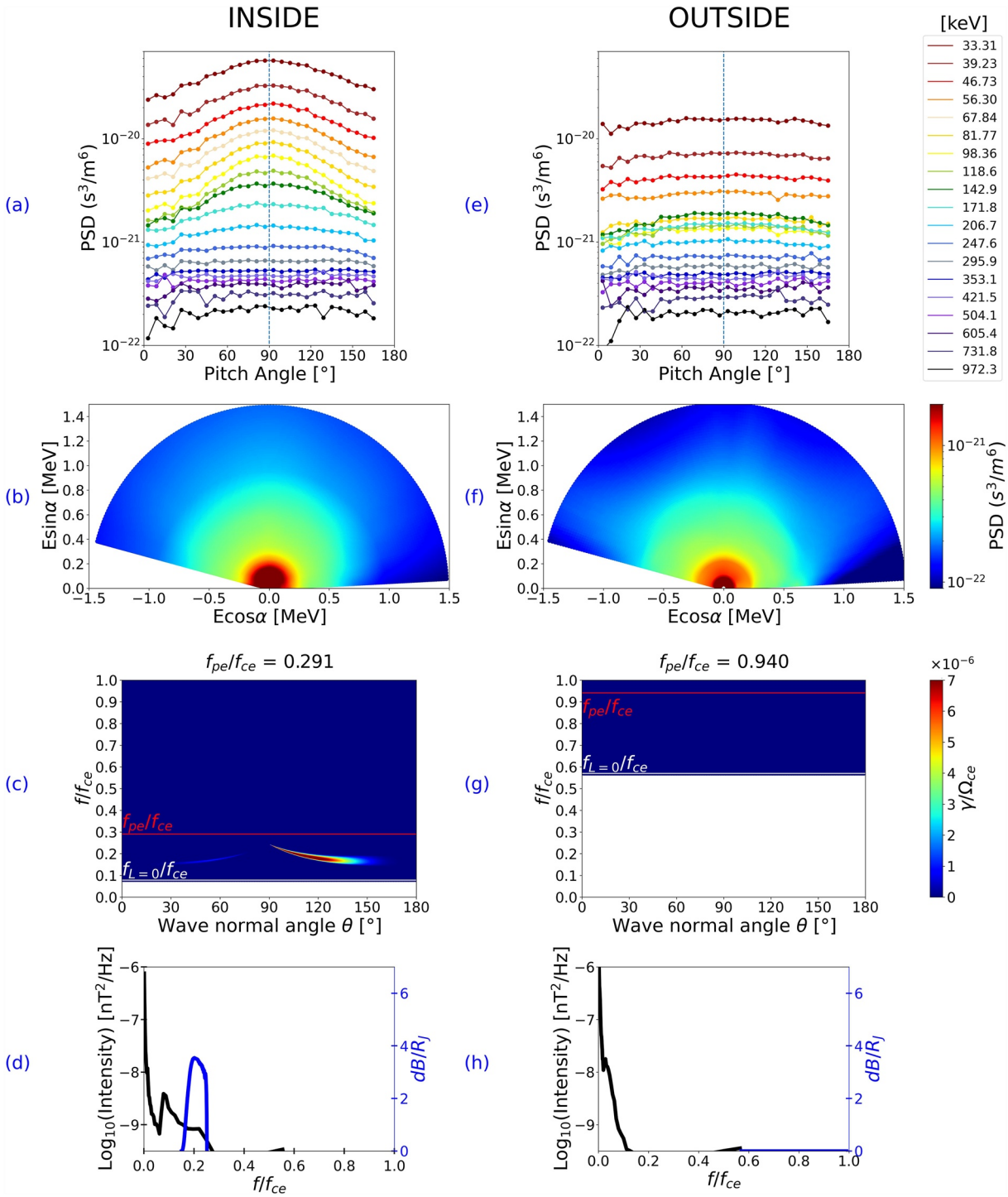

Figure 3. Growth rate analysis for the Z-mode wave event using Juno observations of energetic electrons and plasma waves inside the interchange event (12:24:30 UT) and outside the interchange event (12:22:15 UT) on 17 February 2020. (a) Electron phase space density (PSD) as a function of pitch angle from 33 to 972 keV; (b) Distribution of electron PSD in the parallel and perpendicular energy space; (c) Normalized growth rate of Z-mode waves as a function of wave normal angle and normalized frequency. (d) Observed magnetic wave intensity (black) and convective growth rate in decibels per Jovian radii (blue) as a function of normalized frequency. (e)–(h) The same format as panels (a)–(d) but at 12:22:15 UT outside of the interchange event. f_{pe}/f_{ce} = 0.29 (0.94) inside (outside) of the event.

2. The reported two interchange events associated with whistler-mode waves occurred at *M*-shell ~9, near the equator (MLATs of 15° and 9.1°), and on the nightside (MLTs of 0.8–0.9 hr). These events are indicative of inward radial transport, characterized by an increase in magnetic field strength at the onset of the event, a rapid

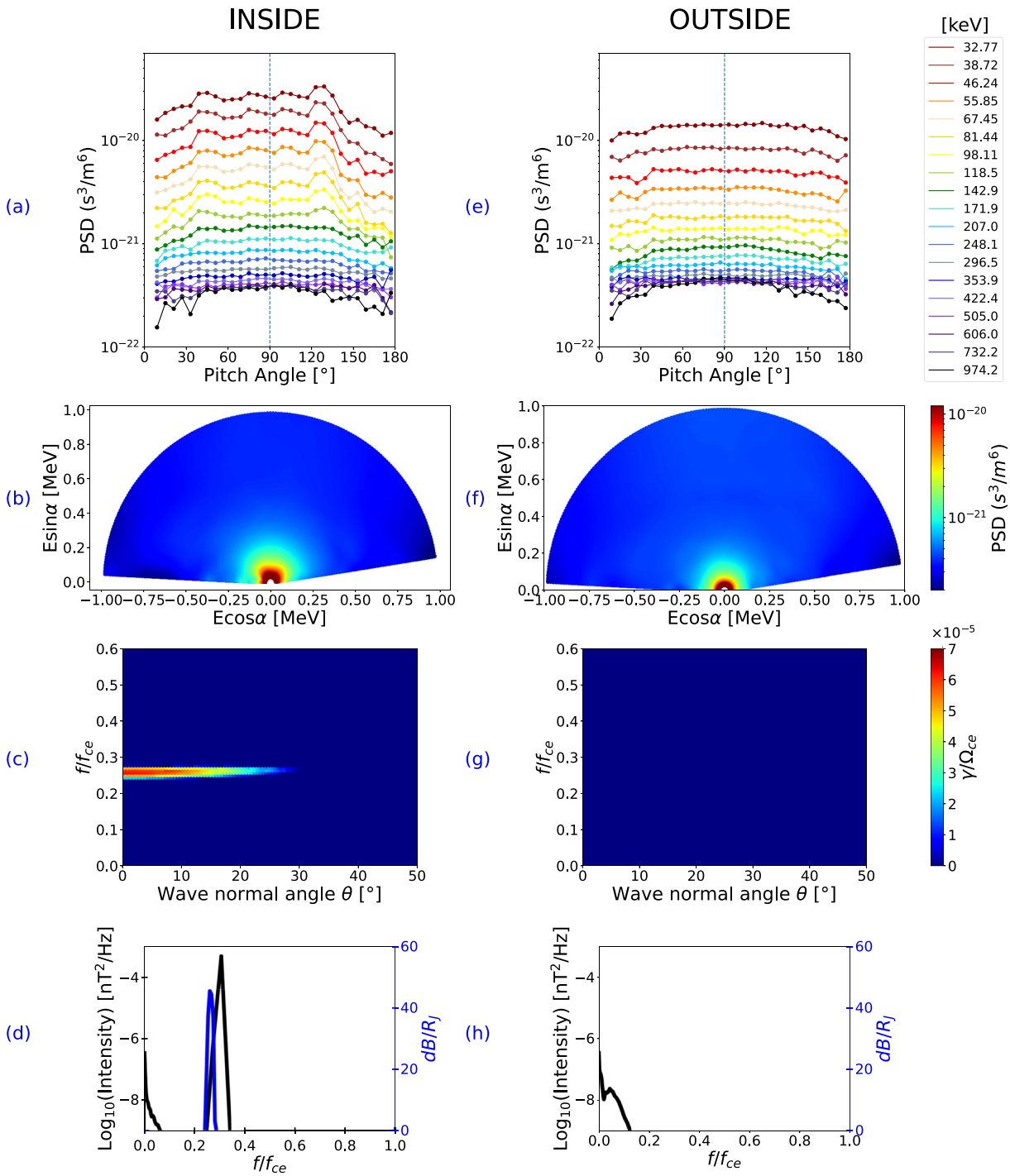

Figure 4. The same format as Figure 3 but for the whistler-mode wave event inside (outside) of interchange event at 06:09:45 UT (06:08:15 UT) on 6 April 2019.

increase in electron flux below hundreds of keV, and a decrease in total electron number density in association with intensification of whistler-mode waves inside of the interchange events.

3. The relativistic linear growth rate of the Z-mode waves peaks over the frequency range of 0.15–0.25 f_{ce}, which is roughly consistent with the observed wave frequency range. This suggests that the intensified Z-mode waves inside of the interchange event are likely locally generated due to the anisotropic distribution of electrons.
4. The relativistic linear growth rate of the whistler-mode waves peaks over the frequency of 0.24–0.28 f_{ce}, which is roughly consistent with the observed lower-band wave frequency range. This feature suggests

that the lower-band waves are locally generated due to the anisotropic distribution of energetic electrons. However, further investigations are required to explain the generation of the upper-band waves, which are highly electrostatic.

To comprehensively assess the distribution of interchange events associated with specific plasma waves, a systematic analysis covering a wider region that may be favorable for the generation of various wave modes would be valuable. However, such an extensive analysis goes beyond the scope of the present study. Nonetheless, our study regarding the analysis of interchange events associated with plasma waves, using the combined Juno observations and theoretical growth rate calculations, reveals the key characteristics of interchange events and the generation of associated plasma waves (Z-mode and whistler-mode). These findings improve our understanding of the fundamental question regarding the generation of whistler-mode and Z-mode waves and provide valuable insights into the particle transport and the associated plasma wave generation in the Jovian magnetosphere and other magnetized environments.

Data Availability Statement

The Juno Waves data are publicly available in NASA Planetary Data System (PDS) via https://doi.org/10.17189/1520498 (Kurth & Piker, 2022), JEDI data are publicly available in NASA PDS via https://doi.org/10.17189/1519713 (Mauk, 2022), JADE data are publicly available in NASA PDS via https://doi.org/10.17189/1519715 (Allegrini et al., 2022), and Magnetometer data are publicly available in NASA PDS via https://doi.org/10.17189/1519711 (Connerney, 2022). We acknowledge Wilson et al. (2023) for the use of the Jovian magnetic field model. The data used to produce figures in the present study are publicly available in figshare via https://doi.org/10.6084/m9.figshare.20988010.

Acknowledgments
The research at Boston University is supported by the NASA Grant 80NSSC20K0557 and Subcontract Q99064JAR under NASA Prime contract NNM06AA75C. QM acknowledges the subcontract 699046X to UCLA under prime contract ZZM06AA75C, the NASA Grant 80NSSC20K0196, and the NSF Grant AGS-2225445. The research conducted by P.H.Y. was supported by NSF Grants 2203321 and the Department of Energy Award DE-SC0022963 through the NSF/DOE Partnership in Basic Plasma Science and Engineering and NASA Grant 80NSSC23K0662. The research at the University of Iowa is supported by NASA through Contract 699041X with the Southwest Research Institute. WSK acknowledges the use of the Space Physics Data Repository at the University of Iowa supported by the Roy J. Carver Charitable Trust. J. D. Menietti Acknowledges NASA Grant 80NSSC19K1262.

References

Allegrini, F., Wilson, R. J., Ebert, R. W., & Loeffler, C. (2022). JUNO J/SW JOVIAN AURORAL DISTRIBUTION CALIBRATED V1.0, JNO-J/SW-JAD-3-CALIBRATED-V1.0 [Dataset]. NASA Planetary Data System. https://doi.org/10.17189/1519715

Azari, A. (2020). A data-driven understanding of plasma transport in Saturn's magnetic environment, (Doctoral dissertation). *Deep Blue*. https://hdl.handle.net/2027.42/155251

Azari, A. R., Liemohn, M. W., Jia, X., Thomsen, M. F., Mitchell, D. G., Sergis, N., et al. (2018). Interchange injections at Saturn: Statistical survey of energetic H^+ sudden flux intensifications. *Journal of Geophysical Research: Space Physics*, *123*(6), 4692–4711. https://doi.org/10.1029/2018JA025391

Bagenal, F., Dougherty, L. P., Bodisch, K. M., Richardson, J. D., & Belcher, J. M. (2017). Survey of Voyager plasma science ions at Jupiter: 1. Analysis method. *Journal of Geophysical Research: Space Physics*, *122*(8), 8241–8256. https://doi.org/10.1002/2016JA023797

Bolton, S. J. (2010). The Juno mission. *Proceedings of the International Astronomical Union*, *6*(S269), 92–100. https://doi.org/10.1017/S1743921310007313

Bolton, S. J., Thorne, R. M., Gurnett, D. A., Kurth, W. S., & Williams, D. J. (1997). Enhanced whistler-mode emissions: Signatures of interchange motion in the Io torus. *Geophysical Research Letters*, *24*(17), 2123–2126. https://doi.org/10.1029/97GL02020

Burch, J. L., Goldstein, J., Hill, T. W., Young, D. T., Crary, F. J., Coates, A. J., et al. (2005). Properties of local plasma injections in Saturn's magnetosphere. *Geophysical Research Letters*, *32*(14), L14S02. https://doi.org/10.1029/2005GL022611

Chen, L., Thorne, R. M., Jordanova, V. K., & Horne, R. B. (2010). Global simulation of magnetosonic wave instability in the storm time magnetosphere. *Journal of Geophysical Research*, *115*(A11), A11222. https://doi.org/10.1029/2010JA015707

Chen, Y., & Hill, T. W. (2008). Statistical analysis of injection/dispersion events in Saturn's inner magnetosphere. *Journal of Geophysical Research*, *113*(A7), A07215. https://doi.org/10.1029/2008JA013166

Connerney, J. E. P. (2022). Juno MAG CALIBRATED DATA J V1.0, JNO-J-3-FGM-CAL-V1.0 [Dataset]. NASA Planetary Data System. https://doi.org/10.17189/1519711

Connerney, J. E. P., Benn, M., Bjarno, J. B., Denver, T., Espley, J., Jorgensen, J. L., et al. (2017). The Juno magnetic field investigation. *Space Science Reviews*, *213*(1–4), 39–138. https://doi.org/10.1007/s11214-017-0334-z

Dougherty, L. P., Bodisch, K. M., & Bagenal, F. (2017). Survey of Voyager plasma science ions at Jupiter: 2. Heavy ions. *Journal of Geophysical Research: Space Physics*, *122*(8), 8257–8276. https://doi.org/10.1002/2017JA024053

Dumont, M., Grodent, D., Radioti, A., Bonfond, B., & Gérard, J.-C. (2014). Jupiter's equatorward auroral features: Possible signatures of magnetospheric injections. *Journal of Geophysical Research: Space Physics*, *119*(12), 10068–10077. https://doi.org/10.1002/2014JA020527

Hill, T. W., Rymer, A. M., Burch, J. L., Crary, F. J., Young, D. T., Thomsen, M. F., et al. (2005). Evidence for rotationally driven plasma transport in Saturn's magnetosphere. *Geophysical Research Letters*, *32*(14), L14S10. https://doi.org/10.1029/2005GL022620

Hospodarsky, G. B., Sigsbee, K., Leisner, J. S., Menietti, J. D., Kurth, W. S., Gurnett, D. A., et al. (2012). In D. Summers, I. R. Mann, D. N. Baker, & M. Schulz (Eds.), *Plasma wave observations at Earth, Jupiter, and Saturn. In dynamics of the Earth's radiation belts and inner magnetosphere*. American Geophysical Union. https://doi.org/10.1029/2012GM001342

Kaiser, M. L., Desch, M. D., Farrell, W. M., Hess, R. A., & MacDowall, R. J. (1993). Ordinary and Z-mode emissions from the Jovian polar region. *Planetary and Space Science*, *41*(11–12), 977–985. https://doi.org/10.1016/0032-0633(93)90102-8

Kennel, C. (1966). Low-frequency whistler mode. *The Physics of Fluids*, *9*(11), 2190–2202. https://doi.org/10.1063/1.1761588

Kennelly, T. J., Leisner, J. S., Hospodarsky, G. B., & Gurnett, D. A. (2013). Ordering of injection events within Saturnian SLS longitude and local time. *Journal of Geophysical Research: Space Physics*, *118*(2), 832–838. https://doi.org/10.1002/jgra.50152

Kivelson, M. G., Khurana, K. K., Russell, C. T., & Walker, R. J. (1997). Intermittent short-duration magnetic field anomalies in the IO torus: Evidence for plasma interchange? *Geophysical Research Letters*, *24*(17), 2127–2130. https://doi.org/10.1029/97GL02202

Kollmann, P., Paranicas, C., Clark, G., Mauk, B. H., Haggerty, D. K., Rymer, A. M., et al. (2017). A heavy ion and proton radiation belt inside of Jupiter's rings. *Geophysical Research Letters*, *44*(11), 5259–5268. https://doi.org/10.1002/2017GL073730

Kurth, W. S., Hospodarsky, G. B., Fadden, J. B., Sulaiman, A. H., Mauk, B. H., Clark, G., et al. (2023). Evidence of fresh interchange injections related to the interchange instability in the Io torus. https://doi.org/10.5194/egusphere-egu23-4260

Kurth, W. S., Hospodarsky, G. B., Kirchner, D. L., Mokrzycki, B. T., Averkamp, T. F., Robison, W. T., et al. (2017). The Juno waves investigation. *Space Science Reviews*, *213*(1-4), 347–392. https://doi.org/10.1007/s11214-017-0396-y

Kurth, W. S., & Piker, C. W. (2022). JUNO E/J/S/SS WAVES CALIBRATED SURVEY FULL RESOLUTION V2.0, JNO-E/J/SS-WAV-3-CDR-SRVFULL-V2.0 [Dataset]. NASA Planetary Data System. https://doi.org/10.17189/1520498

Li, W., Shen, X.-C., Menietti, J. D., Ma, Q., Zhang, X.-J., Kurth, W. S., & Hospodarsky, G. B. (2020). Global distribution of whistler mode waves in Jovian inner magnetosphere. *Geophysical Research Letters*, *47*(15), e2020GL088198. https://doi.org/10.1029/2020GL088198

Li, W., Thorne, R. M., Meredith, N. P., Horne, R. B., Bortnik, J., Shprits, Y. Y., & Ni, B. (2008). Evaluation of whistler mode chorus amplification during an injection event observed on CRRES. *Journal of Geophysical Research*, *113*(A9), A09210. https://doi.org/10.1029/2008JA013129

Ma, Q., Li, W., Chen, L., Thorne, R. M., & Angelopoulos, V. (2014). Magnetosonic wave excitation by ion ring distributions in the Earth's inner magnetosphere. *Journal of Geophysical Research: Space Physics*, *119*(2), 844–852. https://doi.org/10.1002/2013JA019591

Ma, X., Delamere, P. A., & Otto, A. (2016). Plasma transport driven by the Rayleigh-Taylor instability. *Journal of Geophysical Research: Space Physics*, *121*(6), 5260–5271. https://doi.org/10.1002/2015JA022122

Mauk, B. (2022). JEDI CALIBRATED (CDR) DATA JNO J JED 3 CDR V1.0 [Dataset]. NASA Planetary Data System. https://doi.org/10.17189/1519713

Mauk, B. H., Haggerty, D. K., Jaskulek, S. E., Schlemm, C. E., Brown, L. E., Cooper, S. A., et al. (2017). The Jupiter energetic particle detector instrument (JEDI) investigation for the Juno mission. *Space Science Reviews*, *213*(1–4), 289–346. https://doi.org/10.1007/s11214-013-0025-3

McComas, D. J., Alexander, N., Allegrini, F., Bagenal, F., Beebe, C., Clark, G., et al. (2017). The Jovian auroral distributions experiment (JADE) on the Juno mission to Jupiter. *Space Science Reviews*, *213*(1–4), 547–643. https://doi.org/10.1007/s11214-013-9990-9

Menietti, J. D., Averkamp, T. F., Kurth, W. S., Imai, M., Faden, J. B., Hospodarsky, G. B., et al. (2021). Analysis of whistler-mode and Z-mode emission in the Juno primary mission. *Journal of Geophysical Research: Space Physics*, *126*(11), e2021JA029885. https://doi.org/10.1029/2021JA029885

Mitchell, D. G., Brandt, P. C., Carbary, J. F., Kurth, W. S., Krimigis, S. M., Paranicas, C., et al. (2015). Injection, interchange, and reconnection. In A. Keiling, C. M. Jackman, & P. A. Delamere (Eds.), *Magnetotails in the solar system*. https://doi.org/10.1002/9781118842324.ch19

Paranicas, C., Thomsen, M. F., Kollmann, P., Azari, A. R., Bader, A., Badman, S. V., et al. (2020). Inflow speed analysis of interchange injections in Saturn's magnetosphere. *Journal of Geophysical Research: Space Physics*, *125*(9), e2020JA028299. https://doi.org/10.1029/2020JA028299

Rymer, A. M., Mauk, B. H., Hill, T. W., André, N., Mitchell, D., Paranicas, C., et al. (2009). Cassini evidence of rapid interchange transport at Saturn. *Planetary and Space Science*, *57*(14–15), 1779–1784. https://doi.org/10.1016/j.pss.2009.04.010

Southwood, D. J., & Kivelson, M. G. (1987). Magnetospheric interchange instability. *Journal of Geophysical Research*, *92*(A1), 109–116. https://doi.org/10.1029/JA092iA01p00109

Thomsen, M. F. (2013). Saturn's magnetospheric dynamics. *Geophysical Research Letters*, *40*(20), 5337–5344. https://doi.org/10.1002/2013GL057967

Thomsen, M. F., Mitchell, D. G., Jia, X., Jackman, C. M., Hospodarsky, G., & Coates, A. J. (2015). Plasmapause formation at Saturn. *Journal of Geophysical Research: Space Physics*, *120*(4), 2571–2583. https://doi.org/10.1002/2015JA021008

Thorne, R. M., Armstrong, T. P., Stone, S., Williams, D. J., McEntire, R. W., Bolton, S. J., et al. (1997). Galileo evidence for rapid interchange transport in the Io Torus. *Geophysical Research Letters*, *24*(17), 2131–2134. https://doi.org/10.1029/97gl01788

Tilley, M. A., Harnett, E. M., & Winglee, R. M. (2016). Extrasolar giant magnetospheric response to steady-state stellar wind pressure at 10, 5, 1, and 0.2 au. *The Astrophysical Journal*, *827*(1), 77. https://doi.org/10.3847/0004-637x/827/1/77

Wilson, R. J., Vogt, M. F., Provan, G., Kamran, A., James, M. K., Brennan, M., & Cowley, S. W. H. (2023). Internal and external Jovian magnetic fields: Community code to serve the magnetospheres of the outer planets community. *Space Science Reviews*, *219*(1), 15. https://doi.org/10.1007/s11214-023-00961-3

Wu, C. S., & Lee, L. C. (1979). A theory of terrestrial kilometric radiation. *The Astrophysical Journal*, *230*, 621. https://doi.org/10.1086/157120

Xiao, F., Thorne, R. M., Gurnett, D. A., & Summers, D. (1998). Instability of electromagnetic R-mode waves in a relativistic plasma. *Physics of Plasmas*, *5*(7), 2489–2497. https://doi.org/10.1063/1.872932

Xiao, F., Thorne, R. M., Gurnett, D. A., & Williams, D. J. (2003). Whistler-mode excitation and electron scattering during an interchange event near Io. *Geophysical Research Letters*, *30*(14), 1749. https://doi.org/10.1029/2003GL017123

Yoon, P. H., & Krauss-Varban, D. (1990). Gyroharmonic maser instability for weakly relativistic electrons with a loss-cone distribution. *Physics of Fluids B: Plasma Physics*, *2*(8), 1918–1927. https://doi.org/10.1063/1.859463

Yoon, P. H., Weatherwax, A. T., & Rosenberg, T. J. (1998). On the generation of auroral radio emissions at harmonics of the lower ionospheric electron cyclotron frequency: *X, O* and *Z* mode maser calculations. *Journal of Geophysical Research*, *103*(A3), 4071–4078. https://doi.org/10.1029/97JA03526